

PAPER • OPEN ACCESS

Superconductivity and electron–phonon interaction in $\text{Sr}_x\text{Bi}_2\text{Se}_3$ under pressure

To cite this article: Mingtao Li *et al* 2021 *New J. Phys.* **23** 083011

View the [article online](#) for updates and enhancements.



PAPER

Superconductivity and electron–phonon interaction in $\text{Sr}_x\text{Bi}_2\text{Se}_3$ under pressure

OPEN ACCESS

RECEIVED
13 May 2021REVISED
29 June 2021ACCEPTED FOR PUBLICATION
15 July 2021PUBLISHED
9 August 2021

Original content from
this work may be used
under the terms of the
[Creative Commons
Attribution 4.0 licence](#).

Any further distribution
of this work must
maintain attribution to
the author(s) and the
title of the work, journal
citation and DOI.

Mingtao Li^{1,7} , Yifei Fang^{2,3,4,7} , Curtis Kenney-Benson⁵ and Lin Wang^{1,6,*} 

- ¹ Center for High Pressure Science and Technology Advanced Research, Shanghai 201203, People's Republic of China
 - ² Innovation and Integration Center of New Laser Technology, Shanghai Institute of Optics and Fine Mechanics, Chinese Academy of Sciences, Shanghai 201800, People's Republic of China
 - ³ Department of Physics, Fudan University, Shanghai 200433, People's Republic of China
 - ⁴ Center of Materials Science and Optoelectronics Engineering, University of Chinese Academy of Sciences, Beijing 100049, People's Republic of China
 - ⁵ High Pressure Collaborative Access Team, X-ray Science Division, Argonne National Laboratory, Lemont, Illinois 60439, United States of America
 - ⁶ Center for High Pressure Science (CHiPS), State Key Laboratory of Metastable Materials Science and Technology, Yanshan University, Qinhuangdao, Hebei 066004, People's Republic of China
 - ⁷ Authors contributed equally to this work.
- * Author to whom any correspondence should be addressed.

E-mail: linwang@ysu.edu.cn**Keywords:** superconductivity, Raman-scattering, electron–phonon interaction, topological materialSupplementary material for this article is available [online](#)**HPSTAR
1246-2021****Abstract**

Pressure-induced superconductivity has been widely explored and observed in Bi_2Se_3 -based topological materials to hunt for topological superconductors. Although their triggered superconductivity has a close connection to their pressure-induced structural phase transitions, the quest for the electron pairing mechanism of these superconducting semiconductors in both their initial rhombohedral and high-pressure phases remains unknown. In this work, we present a systematic study of the pressure effect on superconducting properties and lattice dynamics using a combination of electrical transport, Raman-scattering, and synchrotron x-ray diffraction measurements using diamond anvil cells. One key finding is our observation of a cooperative connection between the strength of the electron–phonon interaction (EPI) generated by optical branches and the pressure-tunable superconductivity in rhombohedral $\text{Sr}_x\text{Bi}_2\text{Se}_3$ crystal. The underlying suppression mechanism of the T_c by pressure is ascribed to the weakening of the electrons' interaction with the optical phonon modes in the rhombohedral phase. In the intermediate monoclinic phase, the T_c value underwent a sharp increase with carrier density accumulation accompanying the concurrent enhanced EPI. This is intuitively unusual since it is expected that the EPI shall be weakened by inducing more conducting carriers in a normal metal. In the tetragonal phase, the superconductivity is interpreted within BCS theory, since it is fully metallized and obeys the adiabatic Born–Oppenheimer approximation well. Our findings are important to fully understand unconventional superconductivity and the unusual pairing mechanism in the layered rhombohedral Bi_2Se_3 -based superconductors.

1. Introduction

The electron–phonon interaction (EPI) is practically and fundamentally important to understand the underlying mechanism of condensed matters [1–3], such as thermoelectricity [4], superconductivity [5–7] and charge-density wave [8, 9]. In conventional BCS superconductors, the EPI is responsible for the formation of Cooper pairs [10], i.e. the bosonic bound states of electrons that are realized by the exchange of longitudinal acoustic phonons. Nevertheless, the observation of superconductivity in doped semiconductors and semimetals challenges the classical BCS pairing regime. The main underlying difficulty

is that the charge-carrier density in these materials is commonly low, thus, involving a low Fermi energy E_F , which is comparable or even smaller than the characteristic phonon frequency (ω_D) [11–14]. This causes the so-called antiadiabatic limit of EPI ($\omega_D/E_F \geq 1$), namely, the energy and momentum relaxation of electrons is slow relative to ω_D . The dominant electron–phonon scattering mechanisms will involve long-wavelength phonons ($q \rightarrow 0$) as expected [1], given that the carriers in semiconductors or semimetals are typically confined within a narrow energy range near E_F . However, it was recently argued that the electronic states away from the Fermi surface (FS) could dominantly contribute to superconductivity pairing in some low-carrier density superconductors [12]. Thus, the pairing mechanism of low-carrier density superconductors remains a challenging and debated issue [11–14].

Pressure is an effective and clean tool to tune the structural and physical properties in various matters [15, 16], providing helpful insights to unravel the nature of emergent quantum states. Recently, pressure-induced superconductivity has been explored and observed in amounts of tetradymite topological materials, including Bi_2Se_3 -based [17–19], Bi_2Te_3 -based [20–24], Sb_2Te_3 [25], and other alloyed materials [26–28] during the search for topological superconductors [29, 30]. In addition, the pressure effect on the T_c and superconductivity was also reported in topological superconductor candidates $M_x\text{Bi}_2\text{Se}_3$ ($M = \text{Cu}, \text{Nb}, \text{Sr}$) [31–34]. Basically, one common feature is that the occurrence of superconductivity involves the pressure-induced structural phase transitions (SPTs). However, the pairing mechanism is rarely discussed despite the unconventional feature of pressure-induced superconducting phases being proposed [17, 21]. In this context, the polar p -wave pairing state is suggested for the ambient phase and high-pressure phase in Bi_2Se_3 -based superconductors, as depicted by the unusually large upper critical field and its quasi-linear temperature dependence [17, 31, 33]. This is difficult to interpret by single-band orbital-limited Werthamer–Helfand–Hohenberg (WHH) theory [35]. The polar p -wave superconductivity seems to be able to capture the main feature of the upper critical field versus temperature for Bi_2Se_3 -based superconductors [17, 19, 28, 33, 36]. However, according to our recent reports in $\text{Nb}_x\text{Bi}_2\text{Se}_3$ [37], we cannot ignore multiband superconductivity scenario to explain the unusually large value of the normalized upper critical field. At ambient conditions, a multiband gap in the superconducting state was recently observed in the $\text{Sr}_x\text{Bi}_2\text{Se}_3$ and $\text{Nb}_x\text{Bi}_2\text{Se}_3$ superconductors [38, 39]. Using angle-resolved photoemission spectroscopy (ARPES) [40], Han *et al* showed that the $\text{Sr}_x\text{Bi}_2\text{Se}_3$ superconductor is a weakly electron-doped semiconductor by Sr dopants. For instance, the carrier density of $\text{Sr}_x\text{Bi}_2\text{Se}_3$ is only in an order of $\sim 10^{19} \text{ cm}^{-3}$ but the T_c is as high as 3 K [41, 42], which classifies it as one of the low carrier-density superconductors. The resultant low Fermi energy makes the conventional BCS theory inappropriate for interpreting the pairing mechanism in rhombohedral $M_x\text{Bi}_2\text{Se}_3$ superconductors [11, 43].

While the pressure suppresses the T_c values in $\text{Sr}_x\text{Bi}_2\text{Se}_3$ [32, 33], interestingly, Zhou *et al* reported the pressure-induced reemergence of 3.6 K superconductivity at around 6 GPa [33]. The reemergence of superconductivity was ascribed to the SPT from the low-pressure rhombohedral ($R\bar{3}m$) to high-pressure monoclinic ($C2/m$) phase from the XRD patterns [33]. Nevertheless, the pressure-induced reemergence of superconductivity is not confirmed in another study [44]. To the best of our knowledge, the reemergence of superconductivity is not unique, and has been observed in other multiband FeSe-based superconductors [45–47]. While ruling out the appearance of a SPT in pressurized $(\text{Li}_{1-x}\text{Fe}_x)\text{OHFe}_{1-y}\text{Se}$ [47], it was reported that the reemergence of the second high T_c superconducting phase is concomitant with the enhancement of electron-carrier density, indicating an electronic origin, e.g. the pressure-induced FS reconstruction.

As a topological superconductor candidate, the origin of the reemergence of superconductivity and the nature of the high-pressure superconducting phase in $\text{Sr}_x\text{Bi}_2\text{Se}_3$ remains elusive. In this work, we aim to clarify the underlying mechanism of the pressure effect on the T_c , and explore the possible ‘glue-boson’ for the superconducting pairing electrons in pressurized $\text{Sr}_x\text{Bi}_2\text{Se}_3$ crystal. For instance, which type of phonon correlates the superconducting state. Utilizing electrical transport and Hall effect measurements, we confirmed the reemergence of superconductivity with an electronic rather than structural origin. Further, we extracted the physical parameters for the high-pressure phases. Based on these results, we discuss the nature of the superconductivity for the high-pressure phases. BCS theory can explain the superconducting properties of the monoclinic and tetragonal phases. However, this is not the case in rhombohedral phase, which violates the adiabatic limit due to its low-carrier density. Using Raman-scattering, we found compelling evidence of the strong correlation between the strength of the electrons coupled with optical phonons and the superconducting transition temperature. Our results indicate that the pairing is probably mediated by optical phonons, which agrees with the theoretical regimes for the low-carrier density superconductors proposed by Kozii *et al* [11].

2. Experimental methods

A single crystal of nominal $\text{Sr}_{0.12}\text{Bi}_2\text{Se}_3$ was grown by melt method. The source materials with a stoichiometric composition of high-purity metals Sr (2N), Bi (5N) and Se (5N) lumps were loaded into an evacuated ampoule. All the operations were completed in an Ar-filled glovebox with an oxygen and water level below 0.1 ppm. The growth was carried out by slowly cooling the mixture from 1148 K to 900 K at a rate of 2.5 K h^{-1} in a box furnace. After growth, the crystals were annealed at 900 K for more than 24 h and then quenched.

High-pressure electrical transport measurements were carried out using the standard four probes method under van der Pauw configuration in a commercial DynaCool PPMS (QD) [48]. A nonmagnetic BeCu diamond anvil cell (DAC) was used to generate high-pressure conditions. The thin crystals were loaded into a BeCu-DAC with a diamond culet of $300 \mu\text{m}$ (sample size of $\sim 80 \times 80 \times 20 \mu\text{m}^3$). Four pieces of thin platinum foil were utilized as the contacts. Nonmagnetic BeCu alloys with a thickness of $250 \mu\text{m}$ were used as a gasket, and the pre-indented hole was covered by cubic boron nitride (C-BN) as an insulating layer. The samples were put onto the soft NaCl pressure transmitting medium (PTM) with a small ruby ball sitting inside.

The high-pressure synchrotron angle-dispersive XRD of the $\text{Sr}_{0.12}\text{Bi}_2\text{Se}_3$ powder was measured at 16BM-D station (photon energy 30 keV), High Pressure Collaborative Access Team, advanced photon source. A symmetrical Mao-Bell DAC was used to generate high pressure. Mineral oil was used as a PTM. The raw two-dimensional (2D) XRD images were integrated into 1D reflections versus two-theta angles using DIOPTAS [49]. The distance between the sample and detector, and its set-up parameters was calibrated using standard CeO_2 . The XRD patterns were further analyzed by Rietveld refinement using the GASA program package with the user interface EXPGUI [50, 51].

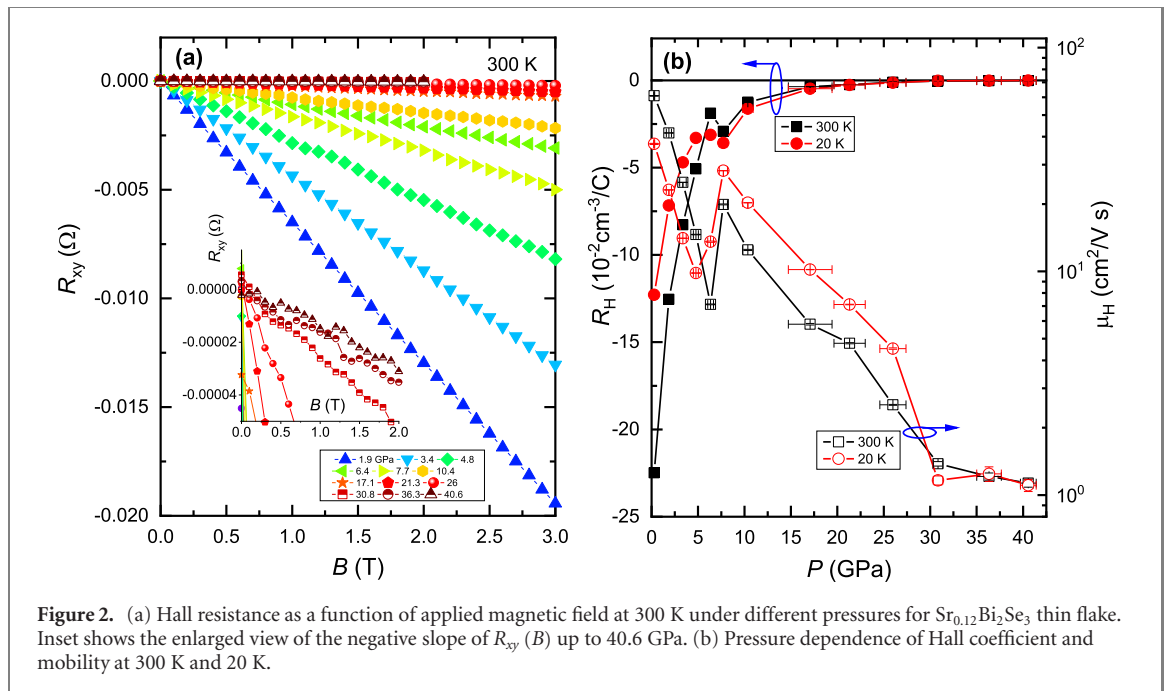
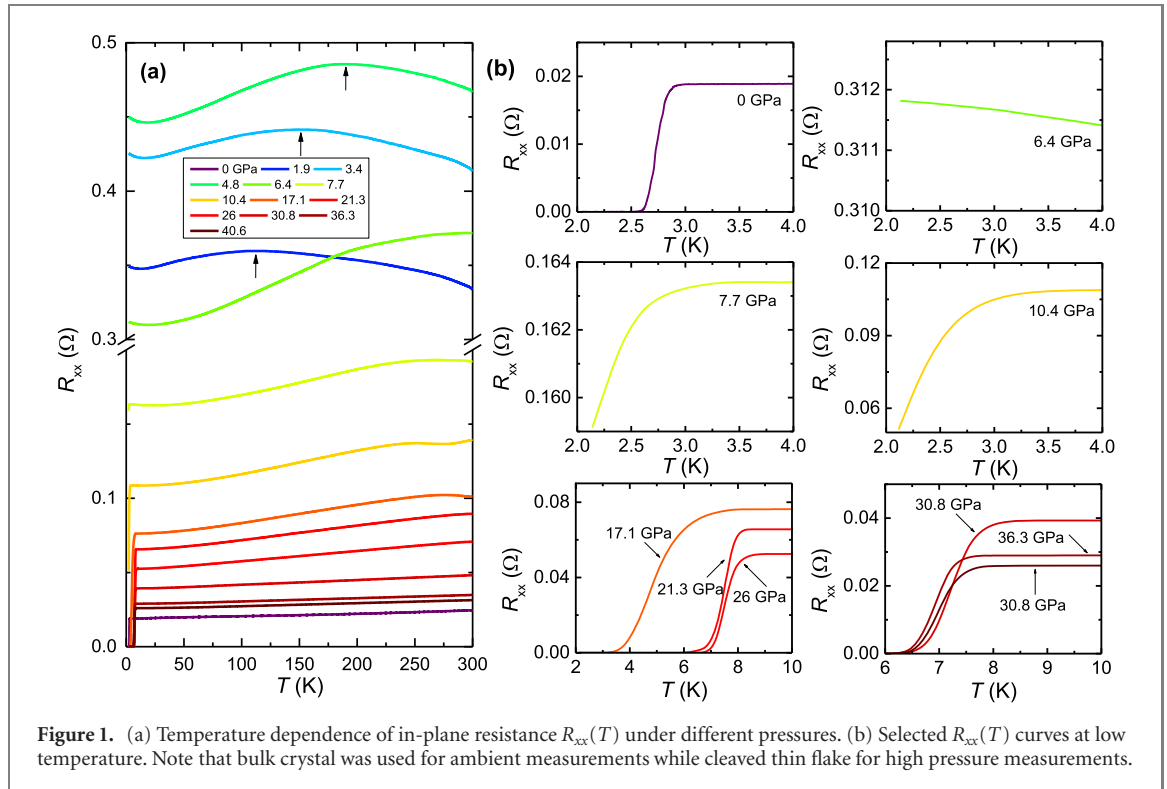
The high-pressure Raman-scattering spectra were measured in a Raman microscope spectrometer (Renishaw, UK) with 633 nm He–Ne laser excitation. A symmetrical Mao-Bell DAC was used to generate high-pressure and mineral oil was used as the PTM. The pressure in all measurements in this work was determined from the standard ruby fluorescence at room temperature [52].

3. Results and discussions

3.1. Reemergent superconductivity and superconducting properties

As shown in figures 1(a) and (b), the as-grown $\text{Sr}_x\text{Bi}_2\text{Se}_3$ crystal has a superconducting transition at around 2.8 K, which is consistent with other reports [41, 42]. However, for the exfoliated thin flake for DAC measurements, the superconducting transition becomes lower ($T_c \sim 2.5 \text{ K}$) and the resistance also shows only a very small drop at 0.28 GPa (not shown). Moreover, the resistivity increases significantly compared to bulk crystal. We attribute it to the decrease of the mobility of thin flake $\text{Sr}_x\text{Bi}_2\text{Se}_3$. For the bulk crystal, the extracted values of the Hall coefficient and mobility at 300 K (20 K) under the ambient pressure were -0.37 (-0.25) cm^{-3}/C and 1284.5 (1057.9) $\text{cm}^2 \text{ V}^{-1} \text{ s}^{-1}$. As seen in figure 2(b), the Hall mobility has around a one order of magnitude decrease for the thin flake. Similar behavior has been observed in the exfoliated thin flakes of Bi_2Se_3 [53] and $\text{Nb}_x\text{Bi}_2\text{Se}_3$ [37]. With applied pressure, the in-plane resistance, $R_{xx}(T)$, of the $\text{Sr}_{0.12}\text{Bi}_2\text{Se}_3$ crystal shows a pronounced increase below 4.8 GPa under different temperatures. One interesting behavior is the appearance of a hump in $R_{xx}(T)$ curves in the pressure range of 0–17.1 GPa with decreasing temperature, as shown in figure 1(a). The hump temperature tends to shift toward high temperature as loading pressure, as indicated by arrows in figure 1(a). This hump might be related to the synergetic contribution of the topological metallic surface state and bulk insulating state to the conductance, as demonstrated in other tetradymite topological insulators [27, 54, 55]. Nevertheless, given the fact that $\text{Sr}_{0.12}\text{Bi}_2\text{Se}_3$ sample is a heavily doped semiconductor, the normal state electrical conduction should be largely dominated by the bulk state and the sizable surface contribution is thus not expected. Another feature is the occurrence of a resistivity minimum at low temperature, which is widely observed in tetradymite topological insulators [27, 33, 54, 56], but no consensus has been reached on the origin of this minimum. Unlike $\text{Cu}_x\text{Bi}_2\text{Se}_3$ [57–59] and $\text{Nb}_x\text{Bi}_2\text{Se}_3$ [37], we found the $R_H(T)$ in $\text{Sr}_{0.12}\text{Bi}_2\text{Se}_3$ bulk crystal shows an unusual nonlinear concave increase down to 10 K at ambient pressure, in good agreement with previous reports [41, 42], implying that conductivity is involved in complicated multi-relaxation rates. This may indicate a multiple electronic band structure [60, 61], reminiscent of the case in Nb-doped Bi_2Se_3 bulk crystals [37, 60].

As shown in figure 1(a), the $R_{xx}(T)$ starts to decline dramatically above 4.8 GPa and decreases until the pressure reaches 40.6 GPa. At 7.7 GPa, a small resistance dip at around 2.57 K is observed, signaling the appearance of superconductivity. At 10.4 GPa, the resistance drop percentage increases for the growing



superconducting region. Thus, our results confirm the reemergence of superconductivity in $\text{Sr}_x\text{Bi}_2\text{Se}_3$ reported by Zhou *et al* [33]. At 17.1 GPa and above, the resistance drops sharply to zero, suggesting a bulk superconducting state was achieved.

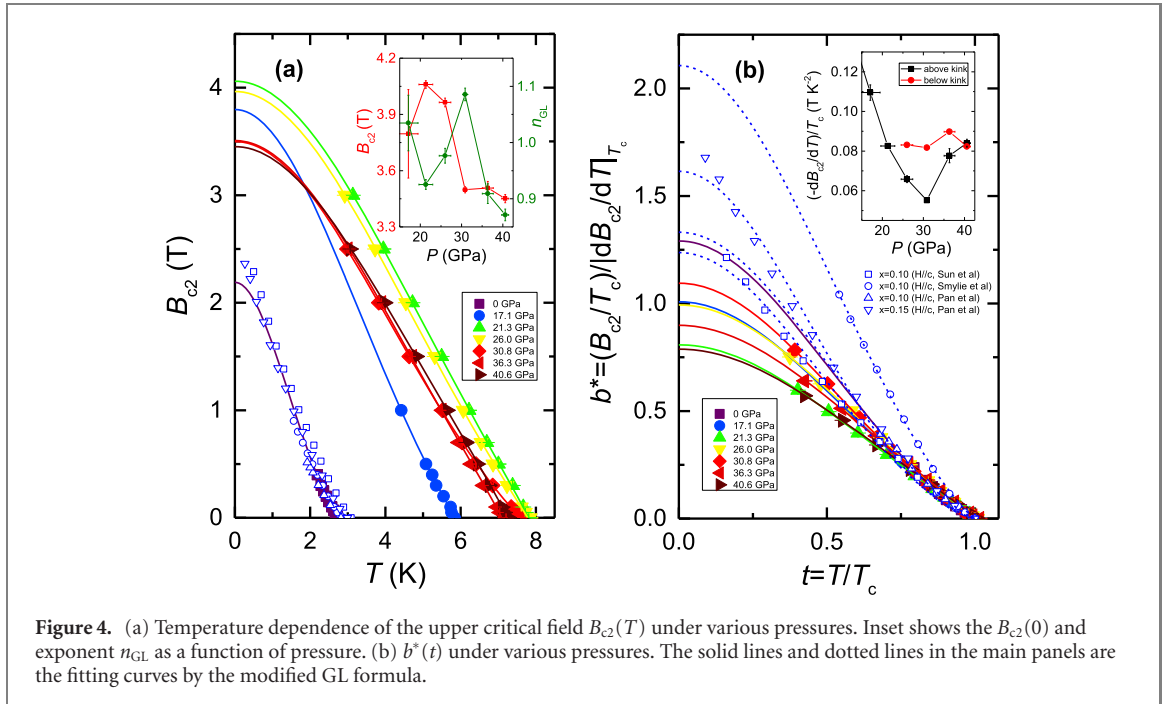
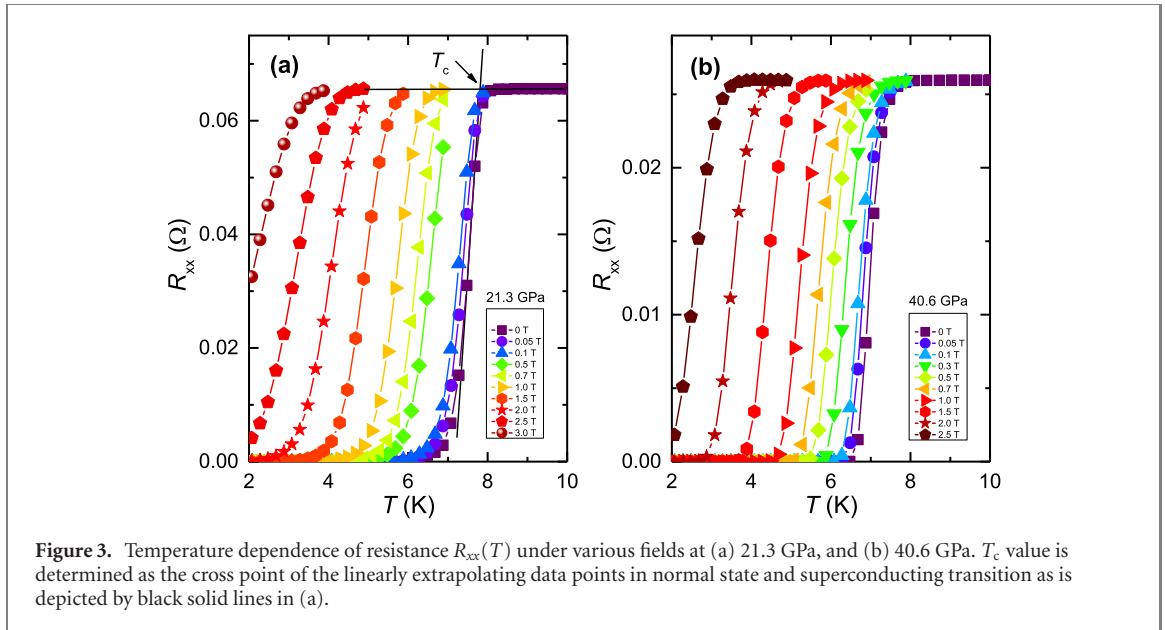
To probe the underlying changes in the electronic band structure, we measured the Hall effect at different pressures under van der Pauw configuration. As shown in figure 2(a), the Hall resistance (R_{xy}) versus the applied field (B) at 300 K shows a linear field dependence with negative slopes. This indicates the dominant electron-type (n -type) carriers up to 40.6 GPa. The symmetrized $R_{xy}(B)$ was obtained by the subtraction of the difference in Hall resistance at positive and negative fields to eliminate the longitudinal contribution [37, 48], and the Hall mobility μ_H was determined accordingly. Figure 2(b) shows the R_H and μ_H as a function of pressure at 300 K and 20 K. On one hand, the $R_H(P)$ shows a similar increase to the loading pressure below around 6.4 GPa (300 K), like Bi_2Se_3 [17, 56]. On the other hand, the curvature of

$R_H(P)$ between the Sr-doped and pure Bi_2Se_3 seems to be different, i.e. concave and convex for the two systems, respectively. This reflects the contrasting electronic band structure of $\text{Sr}_x\text{Bi}_2\text{Se}_3$ induced by Sr dopants. However, a sharp decrease occurs above 6.4 GPa, reaching a minimum at around 7.7 GPa, above which it increases quickly and attains saturation when $P > 30.8$ GPa. In contrast, a decrease of $R_H(P)$ is reported in transition metal-doped $\text{Cu}_{0.30}\text{Bi}_{2.1}\text{Se}_3$ up to 2.31 GPa [31] and $\text{Nb}_{0.25}\text{Bi}_2\text{Se}_3$ up to 7.6 GPa [37]. Meanwhile, the $\mu_H(P)$ below 7.7 GPa at 300 K shows a clear V-shape character with a valley at around 6.4 GPa, above which a dramatic increase occurs. This signals an abrupt change of the FS topology. According to our previous investigations on $\text{Nb}_{0.25}\text{Bi}_2\text{Se}_3$ [37], the observed electronic anomaly in $\text{Sr}_{0.12}\text{Bi}_2\text{Se}_3$ at around 6.4 GPa is likely attributed to the pressure-induced FS reconstruction. Here, we must emphasize that the electronic anomaly observed in pure Bi_2Se_3 at around 8 GPa originates from the SPT supported by the appearance of new reflections in XRD patterns [56]. However, it is attributed to the isostructural electronic anomaly in $\text{Sr}_{0.12}\text{Bi}_2\text{Se}_3$. As discussed later in sections 3 and 4, our synchrotron XRD and Raman-scattering measurements rule out any SPTs below 11 GPa. Benefiting from the slight increase of electron-carrier density induced by Sr doping, the Fermi level is demonstrated to be lifted up compared to pure Bi_2Se_3 [40]. This potentially causes more than one electronic bands cross the Fermi level, thus making $\text{Sr}_x\text{Bi}_2\text{Se}_3$ possess a multiple band feature. The unusual nonlinear convex increase of $R_H(T)$ further supports that multiple bands are at play in $\text{Sr}_x\text{Bi}_2\text{Se}_3$ bulk crystals, which is also shown in references [41] and [42].

The upper critical field versus temperature $B_{c2}(T)$ has been reported in previous reports both at ambient pressure [42, 62–64] and at high pressures on $\text{Sr}_x\text{Bi}_2\text{Se}_3$ bulk crystals [32, 33]. A clear upward feature in $B_{c2}(T)$ for $B \parallel c$ can be seen in previous reports [32, 42, 62–64], yet it is not well addressed. In our sample, we also observed a similar upward inflection at ambient in $B_{c2}(T)$ for $B \parallel c$. Nikitin reported the $B_{c2}(T)$ data for $B \parallel ab$ below 2.15 GPa under hydrostatic pressure, and the inflection is still observable but weakly suppressed by pressure [32]. Zhou *et al* also investigated the $B_{c2}(T)$ behavior of $\text{Sr}_{0.065}\text{Bi}_2\text{Se}_3$ crystal at 19.5 GPa [33], and found quasilinear $B_{c2}(T)$ when approaching to T_c . This behavior observed in Bi_2Se_3 -based superconductors is described in terms of polar p -wave superconductivity [17, 19, 28, 33, 36]. As the FS approaches the Brillouin zone boundary [65], the $b^*(0)$ is also found to be much enhanced over the value for the isotropic FS. Here, the $b^*(t)$ is defined by $(B_{c2}/T_c)/|dB_{c2}/dT|_{T_c}$. This also accompanies a significant upward curvature near the T_c . Recently, using ARPES and quantum oscillation techniques, the bulk FS of $\text{Sr}_x\text{Bi}_2\text{Se}_3$ is proposed to be a quasi-2D cylinder at Γ point with increasing carrier density [66]. As for its counterpart $\text{Cu}_x\text{Bi}_2\text{Se}_3$, it is also reported that the FS evolves from the ellipsoidal FS at low carrier density ($\sim 10^{17} \text{ cm}^{-3}$) to 2D-like cylindrical FS at high carrier density ($\sim 10^{20} \text{ cm}^{-3}$) [67]. This potentially provides the possibility of the inflection in $B_{c2}(T)$ and enhanced $b^*(0)$ originating from the anisotropic FS regime. However, recent STM measurements indicate there are two superconducting gaps in the $\text{Sr}_x\text{Bi}_2\text{Se}_3$ superconductor at ambient conditions [38]. Consequently, the multiband superconductivity seems likely to be responsible for the inflection in $B_{c2}(T)$ and the enhanced $b^*(0)$ for $\text{Sr}_x\text{Bi}_2\text{Se}_3$.

To investigate the magnetic field effects on superconductivity more quantitatively, we measured the suppression of superconductivity by external fields at high pressures. Figures 3(a) and (b) show two representatives at 21.3 GPa and 40.6 GPa. Here, the T_c value under magnetic field is defined as the cross point of the linear extrapolation of data points in normal state and superconducting transition, as seen in figure 3(a). The $B_{c2}(T)$ can be determined plotting the T_c dependent magnetic field, as shown in figure 4(a). The sharp superconducting transition at 0 T indicates the homogeneous high-pressure phase and the external fields suppress the superconducting transition gradually to lower temperatures. We plot the $B_{c2}(T)$ and the normalized $b^*(t)$ curves in figure 3(b), which also include the ambient $B_{c2}(T)$ data from other reports for comparison [62–64]. To obtain $B_{c2}(T)$ at 0 K, we fitted the $B_{c2}(T)$ data with the modified Ginzburg–Landau (GL) relation [37], $B_{c2}^{\text{GL}}(T) = B_{c2}^{\text{GL}}(0) [(1 - t^2)/(1 + t^2)]^{n_{\text{GL}}}$, where n_{GL} is a constant. All $B_{c2}(T)$ data can be well fitted, and the yielded parameters are plotted in the inset of figure 4(a). The fitted $B_{c2}^{\text{GL}}(0)$ is close to the experimental data at the lowest temperature, indicating the modified GL formula is a good approximation for extracting the $B_{c2}(0)$ values. Two key features are revealed in figures 4(a) and (b). Firstly, an upward inflection behavior is consistently observable in the ambient $B_{c2}(T)$ data for all the data points, which is indicative of multiband superconductivity. The upward inflection in $B_{c2}(T)$ manifests in various layered multiband superconductors, such as NbSe_2 [68], MgB_2 [69], and FeSe [70]. Note that the multiband feature is also supported by the observation of an unusual nonlinear concave increase in $R_H(T)$ for the $\text{Sr}_{0.12}\text{Bi}_2\text{Se}_3$ bulk crystal. Recently, we also observed multiband superconductivity in pressurized $\text{Nb}_{0.25}\text{Bi}_2\text{Se}_3$ crystals [37]. Secondly, all the normalized $b^*(t)$ values exceed the $b^*(t) = 0.693(0.727)$ given by the orbital-limited WHH formula in the dirty (clean) limit [35, 71].

Actually, the electron mean free path l under pressures was evaluated to verify the pressurized crystal is in the dirty limit. Assuming a spherical FS, the mean free path can be estimated by $l = \frac{\hbar(3\pi^2n)^{1/3}}{\rho_0 ne^2}$, which is in the range of 0.31–1.12 nm. These values are much smaller than the coherence length ($\xi = 9.01$ – 9.77 nm), supporting the dirty limit situation. Unlike in $\text{Nb}_{0.25}\text{Bi}_2\text{Se}_3$ crystals [37], no clear multiple band feature



characterized by non-linear $R_{xy}(B)$ or a switch of charge-carrier type is observed in the Hall effect measurements for pressurized $\text{Sr}_{0.12}\text{Bi}_2\text{Se}_3$ crystals. Therefore, we cannot totally rule out other sources of enhancing $b^*(0)$ like the anisotropic FS [65]. Overall, given the polar p -wave model or WHH model in single band regime do not yield the upward inflection feature of the $b^*(t)$ for an isotropic FS, multiband superconductivity is a plausible explanation for the unusually large values of $b^*(0)$ in Bi_2Se_3 -based superconductors. The results of two-band fitting on $B_{c2}(T)$ at ambient pressure, 26.0 GPa and 36.3 GPa were given in the supplementary materials (<https://stacks.iop.org/NJP/23/083011/mmedia>), which further supports the multiband superconductivity scenario.

We now turn to discuss the $B_{c2}(0)$ and the slope $|dB_{c2}/dT|_{T_c}$ versus pressure to get more qualitative insights into the superconducting properties. To start with, it is noted the $B_{c2}(0) \propto T_c^2/\nu_F^2$ holds for the isotropic gap single-band superconductor [71]. By including the orbital limited WHH formula, $B_{c2}^{\text{orb}}(0) = 0.693T_c|dB_{c2}/dT|_{T_c}$ in the dirty limit [35], or $B_{c2}^{\text{orb}}(0) = 0.727T_c|dB_{c2}/dT|_{T_c}$ in the clean limit [71], one easily finds the relation $S = |dB_{c2}/dT|_{T_c}/T_c \propto 1/\nu_F^2$ for a single-band superconductor [71], where ν_F is Fermi velocity. For isotropic FS [71], the Fermi velocity is given by $\nu_F = [2E_F^2/\pi^2\hbar^3N(0)]^{1/3} \propto n^{1/3}/m^*$. As shown in the insets of figure 4, a dramatic drop is observed in $B_{c2}(0)$ and an apparent jump in

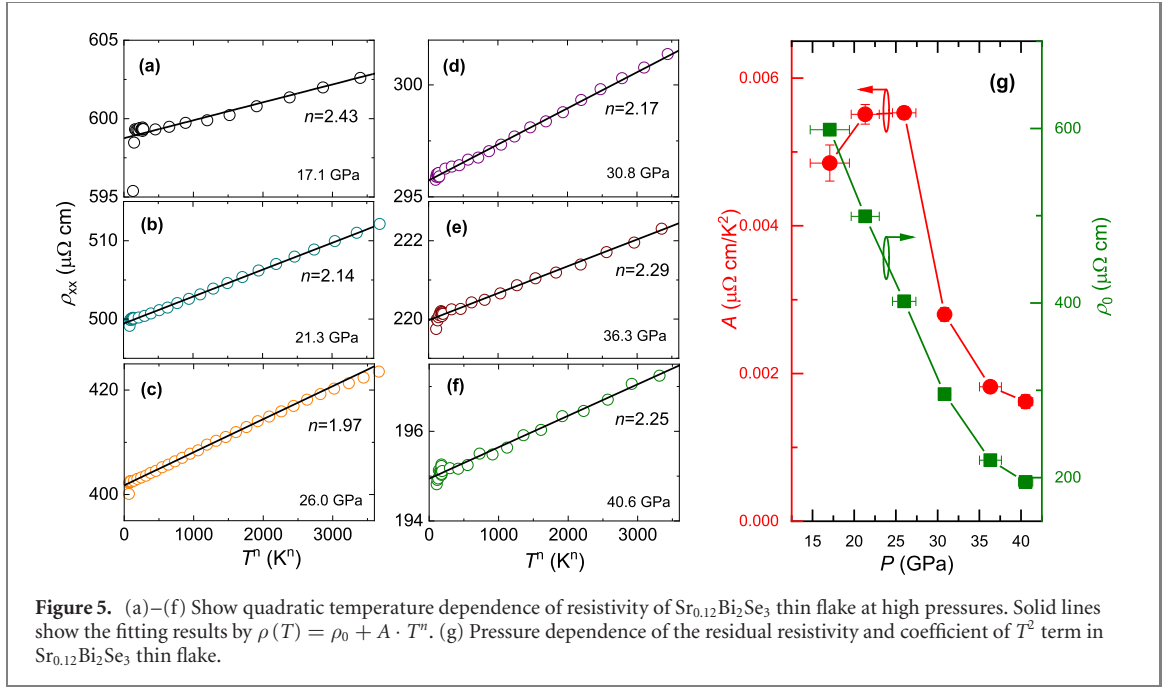


Figure 5. (a)–(f) Show quadratic temperature dependence of resistivity of $\text{Sr}_{0.12}\text{Bi}_2\text{Se}_3$ thin flake at high pressures. Solid lines show the fitting results by $\rho(T) = \rho_0 + A \cdot T^n$. (g) Pressure dependence of the residual resistivity and coefficient of T^2 term in $\text{Sr}_{0.12}\text{Bi}_2\text{Se}_3$ thin flake.

$|dB_{c2}/dT|_{T_c}/T_c$ near the T_c above 30.4 GPa. Also, the second slope above the inflection field further supports the occurrence of a jump, and the criterion for determining the second slope can be found in reference [37]. This strongly signifies the reconstruction of FS, which has the origin of a first-order structure phase transition as demonstrated in section 3. More quantitative analysis on the superconducting parameters can be found in supplementary materials, which has discussed the pressure evolution of the lower critical field $B_{c1}(0)$, thermodynamic critical field $B_c(0)$, electronic specific-heat coefficient γ_s , density of states $N(E_F)$ for $\text{Sr}_{0.12}\text{Bi}_2\text{Se}_3$.

3.2. Normal state properties

In previous studies [17, 19, 26–28, 32, 33], the normal state properties of the high-pressure phases are rarely explored in Bi_2Se_3 -based topological materials. However, the study of the normal state properties can also provide useful information to fully understand the unusual superconducting mechanism at high pressures. Since we have already discussed the ambient and low-pressure phases, we mainly focus here on the high-pressure phases with bulk superconducting state between 17.1 GPa and 40.6 GPa.

We began by checking the electrical transport behavior above but not far from the superconducting transition, namely, below 50 K. Representative in-plane resistivity $\rho_{xx}(T)$ curves are plotted in figures 5(a)–(f). To unveil the possible non-Fermi liquid behavior, which widely exists in unconventional superconductors [47], we fitted the $\rho(T)$ data at low temperature using $\rho(T) = \rho_0 + A \cdot T^n$ between 10 K and 30 K, where n is the exponent. For Fermi liquid, $n = 2$ is expected. The fitting results indicate that the n values range from 1.97–2.43, evidencing the dominant Fermi liquid behavior.

To study the change of coefficient A as a function of pressure, we refitted the $\rho_{xx}(T)$ data by fixing $n = 2$. The results are summarized in figure 5(g). While the residual resistivity drops smoothly, a sharp drop is observed in A between 26 GPa and 30.8 GPa. For heavy fermion compounds, doped insulators/semiconductors, and semimetals [72, 73], the A coefficient is connected to the effective mass m^* by $A \propto (m^*)^2$. The drop of A implies the dramatic decline of the effective mass. Since the Hall coefficient, equivalently the carrier density, simultaneously increases across the pressure from 30.8 GPa to 40.6 GPa, this will cause a decrease in the product of $S \propto 1/\nu_F^2 \propto (m^*/n^{1/3})^2$. However, this is apparently contrary to the experimental result, which shows a clear increase of $\frac{1}{\nu_F^2}$, as displayed in the inset of figure 4(b). Therefore, the simple single band scenario is inadequate to interpret the superconducting properties in the pressurized $\text{Sr}_{0.12}\text{Bi}_2\text{Se}_3$ crystal, hinting the multiband superconductivity.

Moreover, by fitting the normal state $\rho_{xx}(T)$ with broader temperature range using the electron–phonon scattering Umklapp processes model and the Bloch–Grüneisen model (see supplementary materials), the pressure dependence of resistivity determined Debye temperature was obtained. This enables us to evaluate the electron–phonon coupling constant λ using McMillan’s formula [74], $\lambda = \frac{1.04 + \mu^* \ln(\Theta_D/1.45T_c)}{(1 - 0.62\mu^*) \ln(\Theta_D/1.45T_c) - 1.04}$, with a typical value of $\mu^* = 0.13$. The results show $\lambda \lesssim 1$, indicating an intermediate coupling strength for the $\text{Sr}_{0.12}\text{Bi}_2\text{Se}_3$ at ambient and high pressures.

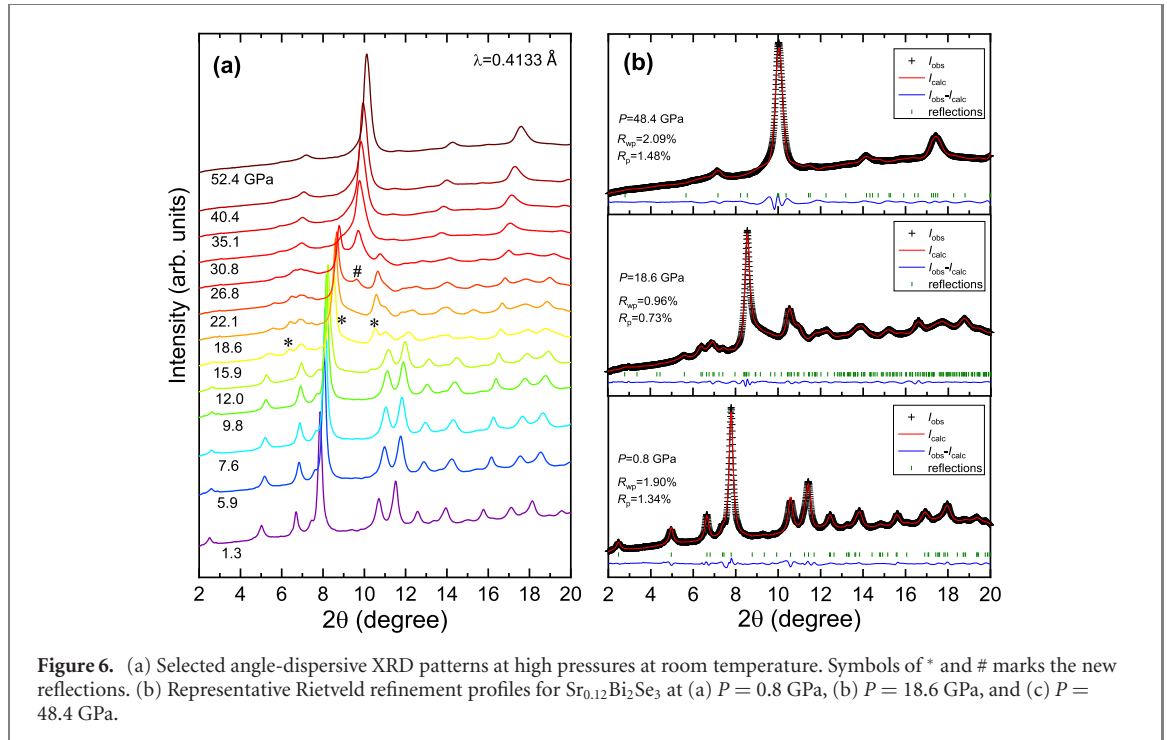


Figure 6. (a) Selected angle-dispersive XRD patterns at high pressures at room temperature. Symbols of * and # marks the new reflections. (b) Representative Rietveld refinement profiles for $\text{Sr}_{0.12}\text{Bi}_2\text{Se}_3$ at (a) $P = 0.8$ GPa, (b) $P = 18.6$ GPa, and (c) $P = 48.4$ GPa.

3.3. Synchrotron x-ray diffraction

It is known that the $\text{Sr}_x\text{Bi}_2\text{Se}_3$ crystal crystallizes into a rhombohedral structure ($R\bar{3}m$, No. 166, CN = 6) like parent Bi_2Se_3 [41]. To understand the pressure-induced superconductivity, a series of synchrotron XRD patterns were measured, as displayed in figure 6(a). We observed two SPTs occurring at around 11 GPa and 20 GPa. According to the previous studies on Bi_2Se_3 [75], $\text{Sr}_x\text{Bi}_2\text{Se}_3$ [33] and $\text{Nb}_x\text{Bi}_2\text{Se}_3$ [37], we further confirm that two high-pressure phases of $\text{Sr}_{0.12}\text{Bi}_2\text{Se}_3$ can be identified as monoclinic (space group: $C2/m$, No. 12, CN = 7) and tetragonal (space group: $I4/mmm$, No. 139, CN = 8) phases. Using the GASA program package with a user interface EXPGUI [50, 51], we refined the XRD patterns for $\text{Sr}_{0.12}\text{Bi}_2\text{Se}_3$ powder and the representative Rietveld refinement profiles at $P = 0.8$ GPa, $P = 18.6$ GPa, and $P = 48.4$ GPa, which are plotted in figures 6(b)–(d). Hereafter, we designate the rhombohedral, monoclinic, and tetragonal phases as the R , M , and T phases, respectively. A series of XRD patterns, refined lattice parameters, the lattice parameter ratio of c/a for R phase, and the volume V/Z versus pressure are plotted in figures 7(a)–(c). The ratio of c/a reaches a broad minimum between 4.6 GPa and 7.6 GPa, above which a jump appears. This contrasts with $\text{Nb}_x\text{Bi}_2\text{Se}_3$ [37], where the c/a undergoes an abrupt drop between 4.9 and 5.4 GPa.

To compare the compressibility with the R phase, we plotted the V/Z versus pressure for the R , M , and T phases in figure 7(c). The $P - V/Z$ data was fitted using the second-order Birch–Murnaghan equation of state (Eos) [76]. The best fitting yielded bulk modulus $K_0^r = 61.0(2.9)$ GPa, its first derivative $K_0^{r,t} = 4$ (fixed) and volume $V_0^r = 142.6(6)$ \AA^3 at ambient pressure for the R phase; $K_0^m = 74.7(16.4)$ GPa, $K_0^{r,m} = 4$ (fixed) and $V_0^m = 131.3(3.8)$ \AA^3 for the M phase; and $K_0^t = 76.6(4.0)$ GPa, $K_0^{r,t} = 4$ (fixed) and $V_0^t = 126.3(1.2)$ \AA^3 for T phase. The volume collapse at the two SPTs is estimated to be 6.42% and 4.62%. In layered materials, the minimum of c/a is commonly attributed to the electronic topological transition (ETT) [75, 77–79]. Recently, we reported the evidence of pressured-induced ETT in the R phase of $\text{Nb}_x\text{Bi}_2\text{Se}_3$ crystal [37], where the hybridization of Nb- $4d$ orbital states and Bi/Se- p orbital states near E_F is at play [39, 60, 80]. According to the first-principle calculations [37], the minimum of c/a can be ascribed to the reconstruction of FS at around 5 GPa benefiting from the lifted Fermi level. We believe a similar transition exists in the $\text{Sr}_x\text{Bi}_2\text{Se}_3$ crystal, where the Fermi level is also lifted due to electron doping by Sr dopants [40]. With increasing pressure around 4.6 GPa, the FS reconstructs. Our results indicate the minimum of c/a may signal an ETT when the Bi_2Se_3 crystal becomes an electron-doped semiconductor by Sr or Nb doping. With applied pressure, the superconductivity is proposed to be associated with the electronic transition at around 7.7 GPa and the SPTs of $R \rightarrow M$ and $M \rightarrow T$ above 12 GPa.

3.4. Raman-scattering

Raman-scattering is a powerful tool to investigate the lattice dynamics of the Raman-active optical phonons at the Γ point [79, 81–88]. Unlike other quantum materials involving magnetic ordering transitions and/or

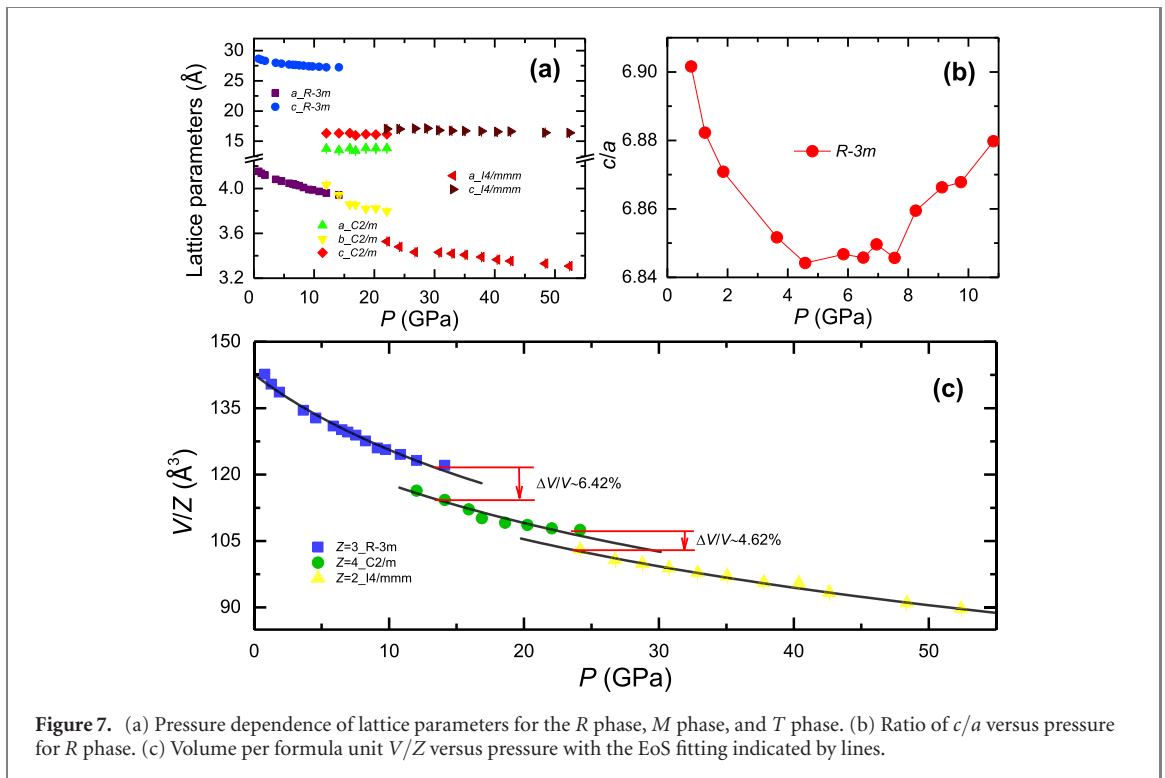


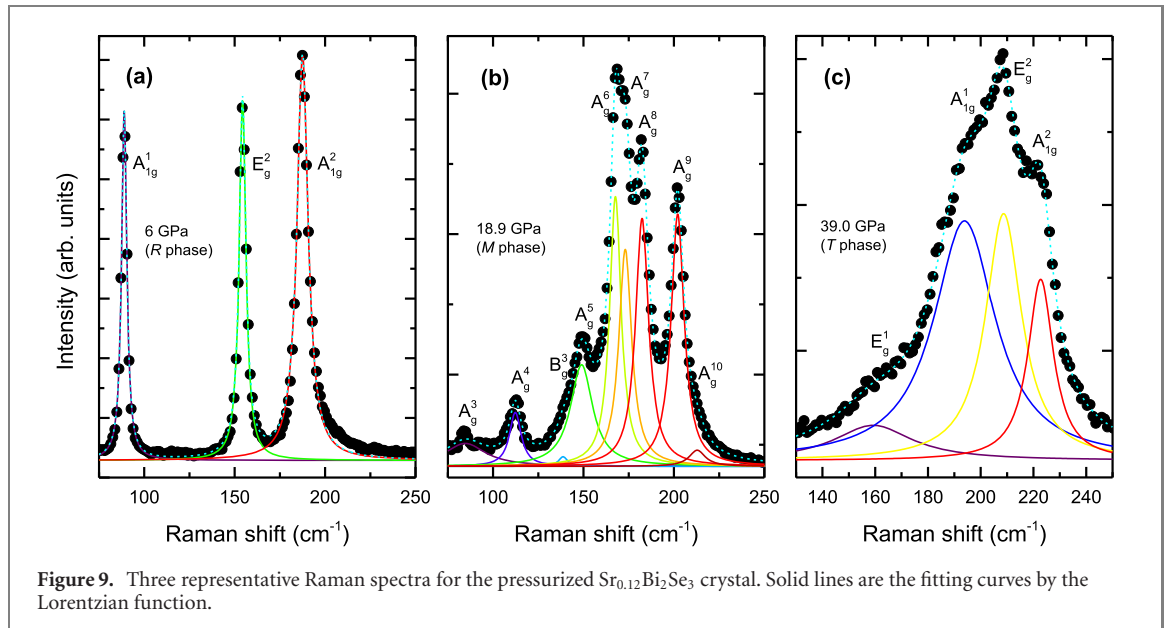
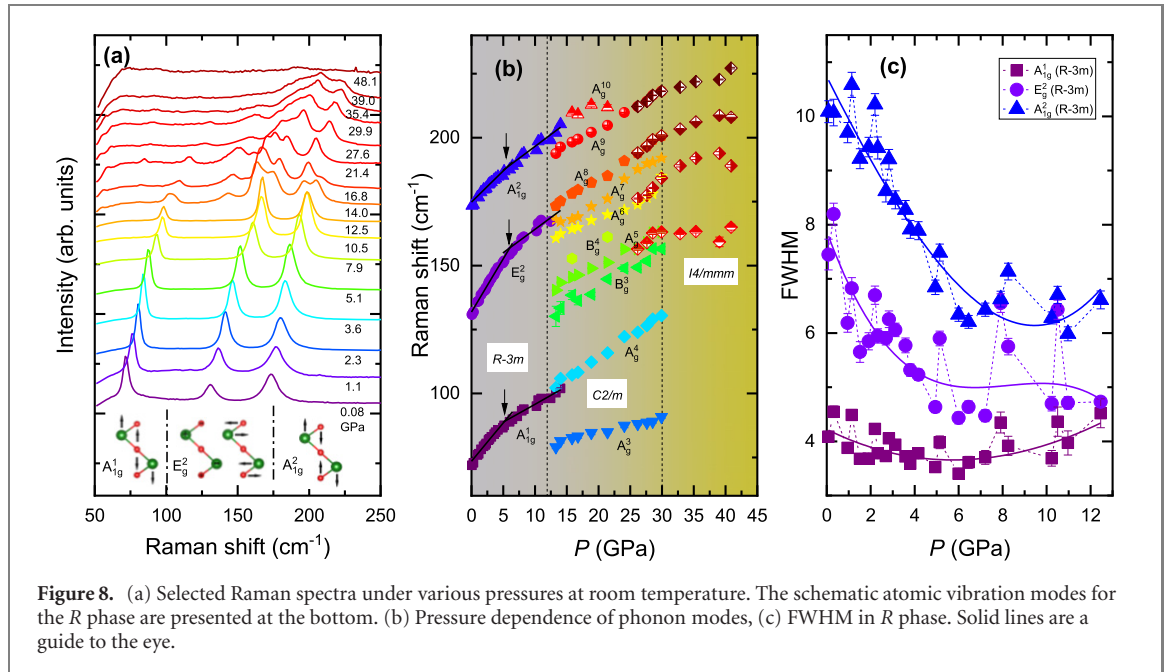
Figure 7. (a) Pressure dependence of lattice parameters for the *R* phase, *M* phase, and *T* phase. (b) Ratio of c/a versus pressure for *R* phase. (c) Volume per formula unit V/Z versus pressure with the EoS fitting indicated by lines.

SPT at low temperature [86, 88], the present studied $\text{Sr}_x\text{Bi}_2\text{Se}_3$ topological material shows no magnetic ordering or SPT with a function of temperature at ambient pressure [41, 42]. This makes it an ideal system to perform an investigation of the pressure effect on the EPI by Raman-scattering, which is definitely helpful for understanding the pairing mechanism in Bi_2Se_3 -based superconductors. For this reason, we carried out the Raman-scattering measurements of the bulk superconducting $\text{Sr}_x\text{Bi}_2\text{Se}_3$ crystal to probe the lattice dynamics at high pressure.

Figures 8(a) and (b) are the pressure dependencies of selected Raman spectrum and the Raman shift ($\omega(P)$). The Raman frequencies are extracted by fitting the spectra using the Lorentzian function. A representative at 6 GPa can be found in figure 9(a). In the *R* phase, according to group theory analysis [37, 79, 89, 90], there are four Raman-active modes ($2A_{1g} + 2E_g$). Experimentally, three of the Raman modes, A_{1g}^1 , E_g^2 , and A_{1g}^2 , were clearly assigned above 50 cm^{-1} , as shown in figure 8(a). Bottom insets of figure 8(a) sketch the corresponding atomic vibration for A_{1g}^1 , E_g^2 , and A_{1g}^2 modes. Briefly, the A_{1g} and E_g modes denote the out-of-plane and in-plane phonon vibrations. The E_g^1 and A_{1g}^1 modes are characterized by the in-phase vibrating for Bi–Se₂ pairs while the opposite-phase is the E_g^2 and A_{1g}^2 modes. Further, one can estimate the Grüneisen parameter using relation $\gamma_G = -\frac{d \ln \omega}{d \ln V} = -\frac{K_0}{\omega} \frac{d \ln \omega}{dP}$, yielding $\gamma_G = 2.16, 1.79, 0.95$ for the A_{1g}^1 , E_g^2 , and A_{1g}^2 modes, respectively.

Similar to Bi_2Se_3 [79], we observed a slope change at around 5 GPa of the three Raman modes in the *R* phase for $\text{Sr}_x\text{Bi}_2\text{Se}_3$, as indicated by the arrows in figure 8(b). According to our previous investigation in $\text{Nb}_x\text{Bi}_2\text{Se}_3$ [37], the origin could be totally different due to the additional electrons doped by Sr. Under pressure [37], the Fermi level shifts down, which may potentially cause an ETT. We will further address this issue in the discussion section. To uncover the pressure-induced electronic anomaly in *R* phase [37, 91], we also plotted the full width at half maximum (FWHM) versus pressure in figure 8(c). Overall, the FWHM of the three phonon modes shows a decrease tendency below 6 GPa. For the A_{1g}^1 mode, an apparent minimum occurs at around 6 GPa while the minimum is not well defined for E_g^2 and A_{1g}^2 modes (see also the second run in supplementary materials). The compression rate change of Raman shift and the reached minimum of FWHM agree with the structural anomalies assigned by XRD, where the ratio of c/a arrives at a broad minimum between 4.6 GPa and 7.6 GPa.

Above 11.0 GPa, additional types of phonon frequencies occur, signifying an SPT from the *R* to *M* phase. This type of pressure-induced change in the Raman phonon modes is commonly observed in Bi_2Se_3 -based materials [37, 79]. Details of the group analysis and assigning the Raman modes can be found in previous reports [37, 79]. As shown in figure 9(b), all the Raman-active modes are observed with a clear blueshift at high pressure above 11 GPa. The four lowest phonon frequencies with symmetry of B_g^1 , A_g^1 , B_g^2 , and A_g^2 are not detected, and their response to pressure remains unknown. The Raman line shape fit was done using the Lorentzian function.



With further increasing pressure, the Raman peaks broadened and weakened more. Above 30 GPa, the phonon frequencies could be fitted by four main frequencies, as shown in figure 9(c), indicating that the second SPT of the $M \rightarrow T$ phase had completed. The Raman peaks of the *T* phase were still observable at 39 GPa in $\text{Sr}_x\text{Bi}_2\text{Se}_3$ but barely detected in $\text{Nb}_x\text{Bi}_2\text{Se}_3$ [37]. This is reasonable since the carrier density at around 40 GPa for $\text{Nb}_{0.25}\text{Bi}_2\text{Se}_3$ is more than two times higher than that of $\text{Sr}_x\text{Bi}_2\text{Se}_3$ at room temperature, which makes its electrostatic-screening more complete. According to the group theory analysis, a total of 15 lattice dynamical modes at Γ point ($q = 0$) are classified, including three acoustic modes composed of one A_{2u} mode and a twofold-degenerated E_u mode. The left are composed of 12 optical modes with irreducible representations expressed by $\Gamma = 2A_{1g} + 2A_{2u} + 2E_g + 2E_u$, in which the *E*-symmetry modes are twofold-degenerated. This indicates there are four Raman-active modes ($2A_{1g} + 2E_g$) with even-parity and four infrared-active modes ($2A_{2u} + 2E_u$) with odd-parity. As shown in figure 9(c), the four Raman modes are clearly assigned by fitting the spectrum using the Lorentzian function.

3.5. Discussions and implications on the pairing mechanism

As seen in figure 10, we summarized the pressure dependence of the T_c and Hall carrier density n_H including previously reported results [32, 33]. The reemergence of superconductivity is confirmed in the *R* phase. However, the T_c increases quickly to its maximum rather than with a sudden jump, as observed

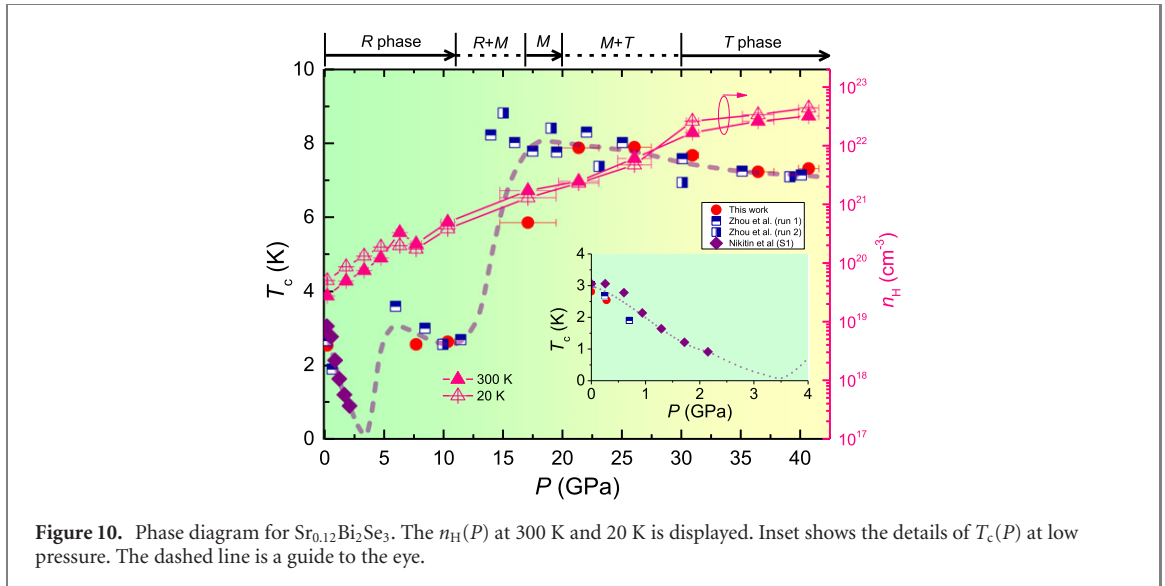
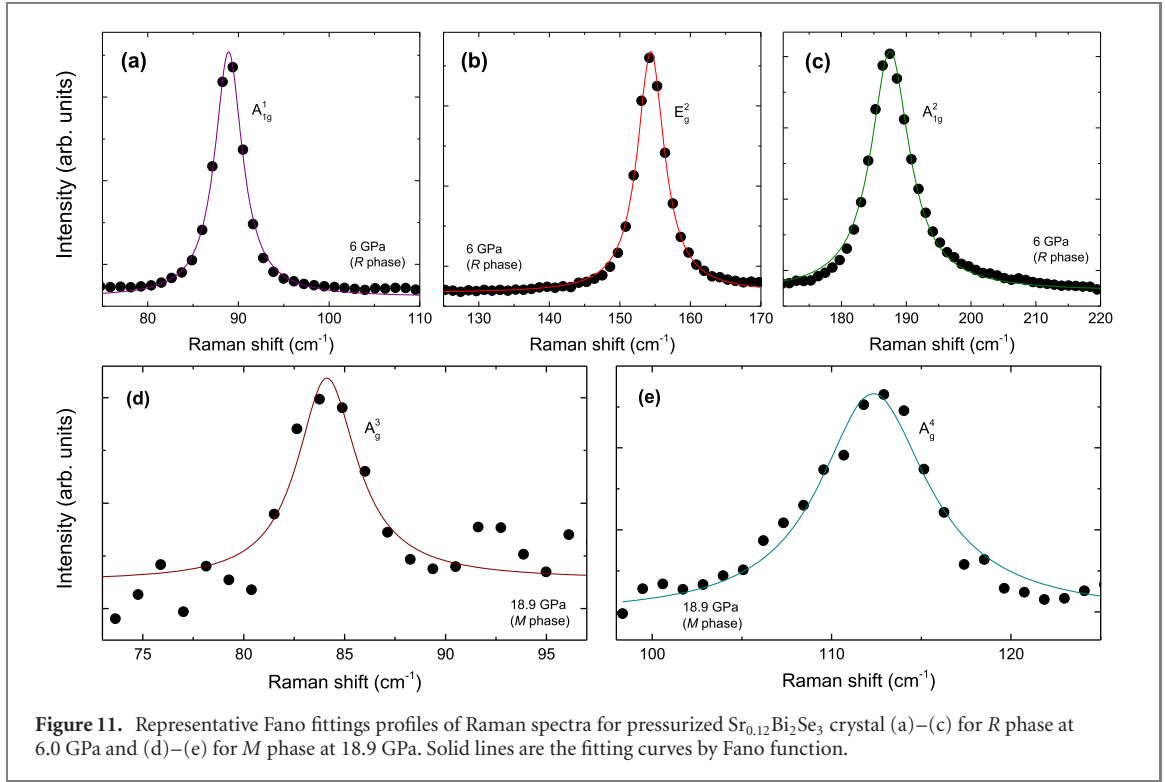


Figure 10. Phase diagram for $\text{Sr}_{0.12}\text{Bi}_2\text{Se}_3$. The $n_{\text{H}}(P)$ at 300 K and 20 K is displayed. Inset shows the details of $T_{\text{c}}(P)$ at low pressure. The dashed line is a guide to the eye.

before [33]. Above 11 GPa, the n_{H} tends to increase up to 40.6 GPa, and the fast increase between 26.0 and 30.8 GPa signals the SPT of the $M \rightarrow T$ phase. Interestingly, below 11 GPa, an anomalously small dip in n_{H} at 300 K seems to occur between 6.4 and 7.7 GPa, which coincides with the broad minimum of c/a , as seen in figure 7(b). This decrease seems to correlate to the reemergence of superconductivity in the R phase. Both our synchrotron XRD and Raman scattering rule out any SPTs below 11 GPa, so the reemergence of superconductivity has its own origin but not the SPT of the $R \rightarrow M$ phase. The abrupt pressure-induced change of n_{H} at around 6.4 GPa indicates an FS reconstruction, probably an ETT, as observed in the pressurized $\text{Nb}_x\text{Bi}_2\text{Se}_3$ crystal [37]. According to the order of n_{H} and μ_{H} during $\text{Sr}_{0.12}\text{Bi}_2\text{Se}_3$ crystal compression, we infer that the M phase and T phase are more like a semimetal and metal, respectively. This speculation is supported by our transverse magnetoresistance (MR) measurement, shown figure S5 in the supplementary materials. In an ordinary metal, the relation of low-field orbital MR is given by $\Delta\rho/\rho(0, T) = [\rho(B, T) - \rho(0, T)]/\rho(0, T) \propto (\omega_c\tau)^2$, where $\omega_c = eB/m^*$ is the cyclotron frequency, m^* is the effective mass of the charge carriers, e is the electrical charge, and τ is the scattering time. Since $\tau = m^*/n\rho_0e^2$ and $\mu = e\tau/m^*$, then the MR is expected to have a quadratic dependence on the product of μB , namely, $\Delta\rho/\rho(0, T) \propto (\mu B)^2$. The $\text{Sr}_x\text{Bi}_2\text{Se}_3$ crystal is actually an electron-doped degenerated semiconductor [40], which has metallic behavior with decreasing temperature. The magnitude of MR in a low magnetic field is sensitive to the order of carrier mobility at a constant field, so the relation of $\text{MR}^T < \text{MR}^M < \text{MR}^R$ is expected for the T , M , and R phases. This is verified by the transverse MR data shown in figure S5, which is consistent with the Hall mobility data in figure 2(b). By establishing the distinguished electronic features for the three phases, their possible superconducting mechanism can be discussed in more detail.

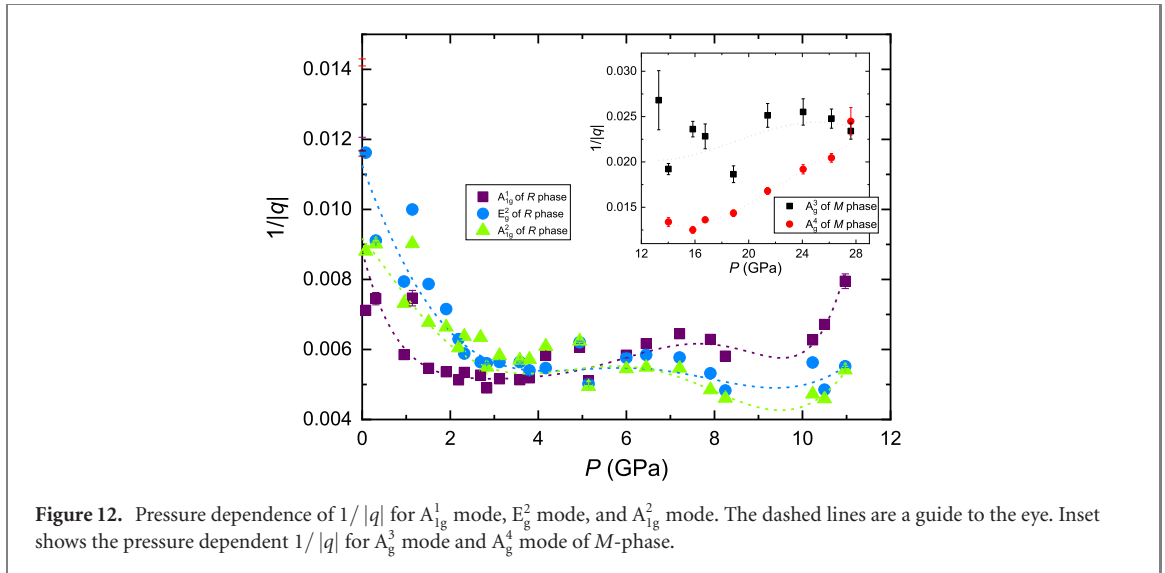
First, we discuss the superconducting mechanism in the T phase of pressurized $\text{Sr}_{0.12}\text{Bi}_2\text{Se}_3$ crystal. As shown in figure 10, the n_{H} has a gradual increase above 30.8 GPa. Meanwhile, the $T_{\text{c}}(P)$ shows a decrease trend simultaneously. The weak suppression of the T_{c} in the T phase can be naturally explained by BCS regime. Importantly, the superconductivity of this phase fully satisfied the adiabatic Born–Oppenheimer approximation (BOA) [92], $\omega/E_{\text{F}} \ll 1$, for the theory of acoustic phonon-mediated superconductivity [10, 11, 82, 93]. To verify this, we calculated the effective mass by the expression $m^* = 3\hbar^2\gamma_{\text{s}}/(V_{\text{mol}}k_{\text{B}}^2k_{\text{F}})$ [59], yielding $m^* = 0.50, 0.81, \text{ and } 0.93 m_{\text{e}}$ for 30.8, 36.3, and 40.6 GPa. The Fermi energy E_{F} was calculated to be 10.16, 7.42, and 7.76 eV, assuming a free electron gas approximation. This results in $\omega/E_{\text{F}} = 2.66 \times 10^{-3}, 3.71 \times 10^{-3}, \text{ and } 3.63 \times 10^{-3}$ by taking the highest frequencies of the $A_{1\text{g}}^2$ mode, and ensuring the validity of the adiabatic BOA for the T phase. According to BCS theory [3, 10], the T_{c} is given by $T_{\text{c}} = 1.14\Theta_{\text{D}} \exp[-1/N(E_{\text{F}})V_0]$ for a phonon-mediated superconductor in weak coupling limit with $N(E_{\text{F}})V_0 = \lambda - \mu^*$, where V_0 is effective electron–electron interaction potential containing an attractive part from EPI and a repulsive electron–electron contribution. On one hand, by fitting $R_{\text{xx}}(T)$ curves in normal state (see supplementary materials), we could evaluate the change of Θ_{D} with pressure, i.e. increasing from 143.13 K at 30.8 GPa to 166.13 K at 40.6 GPa. On the other hand, the increase of n_{H} is expected to result in a decrease of EPI strength for the more complete electrostatic screening. In principle, a concurrent decrease of λ is effective enough to rebalance and suppress the T_{c} due to the dominant exponent term for diminishing T_{c} value. Using McMillan’s formula [74], the λ was calculated to decline from 1.04 at



30.8 GPa to 0.93 at 40.6 GPa, indicating intermediate coupling superconductivity. The weak suppression of the T_c was also observed in the T phase of the pressurized $\text{Nb}_{0.25}\text{Bi}_2\text{Se}_3$ crystal [37]. Combining with McMillan's formula, the pressure dependence of the T_c can be estimated by $d \ln T_c / d \ln V = (-K_0 / T_c) dT_c / dP \cong [-\gamma_G + \Delta \cdot (d \ln \eta / d \ln V + 2\gamma_G)]$ [37, 74, 94], where $\gamma_G = -d \ln \langle \omega \rangle / d \ln V$ is the Grüneisen parameter, $\Delta = 1.04\lambda(1 + 0.38\mu^*) / [\lambda - \mu^*(1 + 0.62\lambda)]^2$, and $\eta = N(E_F) \langle I^2 \rangle$ the Hopfield parameter [95]. Using the bulk modulus $K_0 = 76.6$ GPa by XRD, $dT_c / dP \sim -0.07(2)$ K/GPa (30.0 GPa < P < 36.3 GPa) [33], we obtained $d \ln T_c / d \ln V = (-K_0 / T_c) dT_c / dP = 0.70$. Adopting $d \ln \eta / d \ln V \approx -1$ for the s -electron or p -electron metals [94, 95], and inserting $\lambda = 1.04$, yields a Grüneisen parameter of $\gamma_G = 1.01$ for $\text{Sr}_{0.12}\text{Bi}_2\text{Se}_3$, less than the T phase of pressurized $\text{Nb}_{0.25}\text{Bi}_2\text{Se}_3$ ($\gamma_G = 2.22$) [37] but nearly equal to Bi_2Se_3 ($\gamma_G = 1$) [17]. In comparison with other materials, this value is smaller than those of the transition metals ($\gamma_G \sim 2$ for Nb) [95], MgB_2 ($\gamma_G = 2.36$) [94], and Bi_2Te ($\gamma_G = 1.9$ – 4.38) [24], but comparable to graphite $\gamma = 1.06$ (E_{2g}^2 mode) [96].

Secondly, we discuss the superconducting mechanism in the M phase, which is more like a semimetal. By fitting $R_{xx}(T)$ curves in normal state (see supplementary materials), we evaluated the change of Θ_D with pressure in the M phase, i.e. decreasing from 173.4 K at 17.1 GPa to 134.4 K at 26.0 GPa. However, the increase of n_H observed in the M phase hints at the weakening of EPI intuitively [82]. This would result in severe suppression of the T_c with increasing pressure, which is contradictory to our experimental observation. Therefore, the fast pressure-driven increase of the T_c is unusual in the M phase. While loading pressure from 11.0 to 26.0 GPa, we observed that the $N(E_F)$ increases from 1.70 states/eV-atoms spin per f. u. at 17.1 GPa to 1.99 states/eV-atoms spin per f. u. at 21.6 GPa, followed by a slight decrease to 1.91 states/eV-atoms spin per f. u. at 26.0 GPa. Further, we calculated $\omega / E_F = 3.68 \times 10^{-2}$, 2.57×10^{-2} , and 1.29×10^{-2} by taking the high frequencies of the A_g^9 mode, and ensuring the adiabatic BOA was still valid for the M phase. According to BCS theory [10], the increase of $N(E_F)$ is also effective enough to rebalance and increase the T_c due to the dominant exponent term for improving the T_c value. Again, using McMillan's formula [74], the λ was calculated to increase from 0.83 at 17.1 GPa to 1.10 at 26.0 GPa, which also indicates intermediate coupling superconductivity in the M phase. As discussed below, the unusual enhancement of EPI is also evidenced by the increase of the asymmetric Fano parameter $1/|q|$ versus pressure.

Before discussing the pressure-induced suppression and reemergence of superconductivity in R phase, we need to qualitatively evaluate the strength of the EPI as a function of pressure using Raman-scattering [2]. This can be done by fitting the Raman lines with the standard Fano function [83, 84, 87, 97, 98], which has been commonly adopted to interpret the asymmetric Raman line shapes in semiconductors and superconductors. More details on the fitting can be found in references [43, 83, 84, 87, 97, 98]. The representative fitting profiles by Fano function are shown in figures 11(a)–(e). In our previous study of



Raman-scattering at low temperature [43], we established that the relation, $1/|q| \approx (\pi VT_e/T_p)\rho(\omega)$, is satisfied in the low-carrier density $Sr_xBi_2Se_3$ superconductor at ambient pressure, where q is the asymmetrical parameter, V is anharmonic coefficient describing the electron–phonon coupling matrix element, T_e and T_p are the Raman matrix elements, and $\rho(\omega)$ is the joint density of states of the electronic continuum. Note that this relation is also satisfied and adopted in FeSe-based superconductors [84], which have reported the enhancement of EPI by electron correlation and $\rho(\omega)$ plays a crucial role in determining the T_c . Unlike the M and T phases, the R phase of $Sr_xBi_2Se_3$ is an electron-doped semiconductor. Due to the layered structure and low-carrier density [43], we calculated $\omega/E_F = 2.78$ ($T_F = 89.45$ K in a 2D limit using effective mass $m^* = 0.24m_e$) by taking the high frequencies of the A_{1g}^2 mode at ambient pressure [42, 43, 99]. In addition, using another criterion for validity of BOA, $\omega\tau \ll 1$, it is demonstrated that $\omega\tau = 0.75$ for A_{1g}^2 mode [43]. This indicates the $Sr_xBi_2Se_3$ system violates or is at least close to violating the adiabatic BOA, namely, the antiadiabatic limit is potentially at play in the R phase. The similar situation is also demonstrated in its counterpart, the $Cu_xBi_2Se_3$ ($T_c = 4.18$ K) superconductor [100]. From this aspect, the traditional BCS theory may be inappropriate for describing the superconducting pairing mechanism in the R phase of the $Sr_xBi_2Se_3$ superconductor. Other schemes need to be considered for electrons pairing driven by electron–boson coupling, such as the strong interaction of electrons coupled with the optical phonons [13, 14].

Using Raman-scattering, we demonstrate the optical phonons may indeed play a part in the occurrence of superconductivity in the R phase. To examine the relation between $1/|q|$ and T_c , we extracted the Fano asymmetric parameter $1/|q|$ as a function of pressure, as plotted in figure 12. Intriguingly, we observed a ‘W’-shaped relation of $1/|q|$ versus pressure. The fast suppression of $1/|q|$ by pressure implies the joint density of states declines dramatically, and consequently, the EPI strength decreases. As seen in figure 10, the suppression of the T_c to 0 K is extrapolated to around 3.5 GPa by Niktin *et al* [32], which coincides with the first minimum of $1/|q|$ at around 3.5 GPa. With further increasing pressure, the $1/|q|$ starts to increase and tends to evolve with pressure distinctively at around 5 GPa between A_{1g}^1 mode and the other two modes, above which the $1/|q|$ value of A_{1g}^1 mode exceeds those of the other two modes. This distinct evolution in $1/|q|$ versus pressure evidences the occurrence of ETT, as observed in the electrical transport and synchrotron XRD data. Above 5 GPa, the $1/|q|$ increases again especially for the A_{1g}^1 mode, signaling the increase of EPI. This might be relevant to the reemergence of superconductivity of 3.6 K at around 6 GPa observed by Zhou *et al* [33], and in this work. In our sample, the reemergence of superconductivity is observed at 7.7 GPa, which is somewhat higher than Zhou’s result [33]. Around 7 GPa, the $1/|q|$ begins to decrease, suggesting the decrease of EPI. Meanwhile, the T_c shows ‘V’-shaped behavior between 6.0 and 11.5 GPa. Approaching the $R \rightarrow M$ phase boundary, the fast increase of $1/|q|$ suggests the lattice instability can enhance the EPI. It should be pointed out that, the overall feature of pressure dependent Raman shift, FWHM, and $1/|q|$ can be well repeated in the second run measurements, as seen in the figures S6 and S7 of the supplementary materials. Although the high pressure Raman-scattering data were collected at room temperature, we believe that the behavior of $1/|q|$ versus pressure can be a good reference to that of the R phase at low temperature because there is no SPT down to 10 K for ambient Bi_2Se_3 [101]. Overall, the behavior of $1/|q|$ versus pressure matches the observed $T_c(P)$ for the R phase well, supporting the positive

correlation between EPI and superconductivity. Our results show that the pairing glue can be alternatively mediated by optical phonons, as is theoretically proposed for the low-carrier density superconductors [11].

From a quantitative analysis (see supplementary materials), we demonstrate that the $\text{Sr}_{0.12}\text{Bi}_2\text{Se}_3$ superconductor at ambient pressure processes an unexpectedly larger electronic specific-heat coefficient γ_s than those of high pressure M -phase and T -phase from the upper critical field versus temperature. This is abnormal for the M -phase and T -phase are more metallic. Although the in-plane nematic superconductivity exists in $\text{Sr}_x\text{Bi}_2\text{Se}_3$ and other doped Bi_2Se_3 [62, 102, 103], it may be not relevant to the obtained γ_s value since the $B_{c2}(0)$ was derived with the magnetic field normalized to the ab -plane ($B \parallel c$). According to Wan and Savrasov's theoretical calculations [104], there are large phonon linewidths for both the optical and acoustic modes along the $\Gamma - Z$ direction (at small wave vector q) of the Brillouin zone after electron-doping in Bi_2Se_3 , which originates from the strong EPI. The singular EPI was proposed to arise from the FS nesting [104]. Recently, a large acoustic phonon linewidth was observed in $\text{Sr}_{0.10}\text{Bi}_2\text{Se}_3$ by neutron scattering experiments [105]. The pairing mechanism shows that the calculated s -wave pairing channel of A_{1g} is rather strong and can, in principle, win over other pairing channels without counting the spin-fluctuation effect [105], which is expected to be negligible for the absence of any magnetic ions. In addition, it is evidenced by XRD that the electronic nematicity of $\text{Sr}_x\text{Bi}_2\text{Se}_3$ is closely coupled to the in-plane strain in both the superconducting and normal states [106]. Experimentally, from the scanning tunneling microscopy measurements, strong evidence of s -wave pairing has been reported in $\text{Sr}_x\text{Bi}_2\text{Se}_3$ [38] and $\text{Cu}_x\text{Bi}_2\text{Se}_3$ crystals [107]. Considering the antiadiabatic limit and the observation of the cooperative correlation with the EPI generated by optical phonons and superconductivity of the rhombohedral $\text{Sr}_x\text{Bi}_2\text{Se}_3$ at high pressure, the s -wave pairing mediated by optical phonons needs to be reexamined in doped Bi_2Se_3 superconductors. Finally, we summarized the proposed pairing mechanism for the superconducting Bi_2Se_3 -based materials under pressure in table S3 (see supplementary materials).

4. Conclusions

To summarize, we reported the pressure-induced reemergence of superconductivity, the superconducting properties and lattice dynamics in pressurized $\text{Sr}_x\text{Bi}_2\text{Se}_3$ crystal. According to the results of Hall effect, x-ray diffraction, and Raman-scattering, the origin of the reemergence of superconductivity is an ETT. Raman-scattering demonstrates there is a cooperative connection between the strength of EPI and the pressure-tunable superconductivity in the rhombohedral and monoclinic phases. The weakening of the interaction between the electron with optical phonon modes is responsible for the suppression mechanism of the T_c by pressure in rhombohedral phase within the antiadiabatic limit. This finding indicates the unconventional pairing mechanism associated with optical phonons should be reconsidered in further theoretical modeling for the layered rhombohedral Bi_2Se_3 -based superconductors. In the intermediate monoclinic phase, the sharp increase of the T_c is concomitant with the unusual enhancement of the EPI, while charge-carriers density increases simultaneously. Since the high-pressure tetragonal phase is metallized and well obeys the adiabatic BOA, the superconductivity properties can be understood within the BCS regime.

Acknowledgments

We thank Xueyan Du for technical support. This work is supported by the National Natural Science Foundation of China (Grants Nos. 11804011, 11874076, and 11974112), National Science Associated Funding (NSAF, Grant No. U1530402), and Science Challenging Program (Grant No. TZ2016001). YF is sponsored by Shanghai Sailing Program No. 20YF1455100. Use of the Advanced Photon Source, an Office of Science User Facility operated for the US DOE Office of Science by Argonne National Laboratory, was supported by the US DOE under Contract No. DE-AC02-06CH11357.

Data availability statement

The data that support the findings of this study are available upon reasonable request from the authors.

ORCID iDs

Mingtao Li  <https://orcid.org/0000-0003-1594-8008>

Yifei Fang  <https://orcid.org/0000-0001-5702-9005>

Lin Wang  <https://orcid.org/0000-0001-8276-7026>

References

- [1] Giustino F 2017 *Rev. Mod. Phys.* **89** 015003
- [2] Zhang A-M and Zhang Q-M 2013 *Chin. Phys. B* **22** 087103
- [3] Grimvall G 1976 *Phys. Scr.* **14** 63
- [4] Wang H, Pei Y, LaLonde A D and Snyder G J 2012 *Proc. Natl Acad. Sci.* **109** 9705
- [5] Cheng C, Sun J-T, Liu M, Chen X-R and Meng S 2017 *Phys. Rev. Mater.* **1** 074804
- [6] Rossi M et al 2019 *Phys. Rev. Lett.* **123** 027001
- [7] Timusk T, Porter C D and Tanner D B 1991 *Phys. Rev. Lett.* **66** 663
- [8] Zhang K et al 2018 *Phys. Rev. Lett.* **121** 206402
- [9] Barath H, Kim M, Karpus J F, Cooper S L, Abbamonte P, Fradkin E, Morosan E and Cava R J 2008 *Phys. Rev. Lett.* **100** 106402
- [10] Bardeen J, Cooper L N and Schrieffer J R 1957 *Phys. Rev.* **108** 1175
- [11] Kozii V, Bi Z and Ruhman J 2019 *Phys. Rev. X* **9** 031046
- [12] Gastiasoro M N, Chubukov A V and Fernandes R M 2019 *Phys. Rev. B* **99** 094524
- [13] van der Marel D, Barantani F and Rischau C W 2019 *Phys. Rev. Res.* **1** 013003
- [14] Gor'kov L P 2016 *Proc. Natl Acad. Sci.* **113** 4646
- [15] Gor'kov L P and Kresin V Z 2018 *J. Phys.: Conf. Ser.* **1106** 011001
- [16] Mao H-K, Chen X-J, Ding Y, Li B and Wang L 2018 *Rev. Mod. Phys.* **90** 015007
- [17] Kirshenbaum K et al 2013 *Phys. Rev. Lett.* **111** 087001
- [18] Kong P P et al 2013 *J. Phys.: Condens. Matter.* **25** 362204
- [19] He T et al 2018 *Phys. Rev. B* **97** 104503
- [20] Zhang C, Sun L, Chen Z, Zhou X, Wu Q, Yi W, Guo J, Dong X and Zhao Z 2011 *Phys. Rev. B* **83** 140504
- [21] Zhang J L et al 2011 *Proc. Natl Acad. Sci. USA* **108** 24
- [22] Matsubayashi K, Terai T, Zhou J S and Uwatoko Y 2014 *Phys. Rev. B* **90** 125126
- [23] Jeffries J R, Lima Sharma A L, Sharma P A, Spataru C D, McCall S K, Sugar J D, Weir S T and Vohra Y K 2011 *Phys. Rev. B* **84** 092505
- [24] Stillwell R L, Jenei Z, Weir S T, Vohra Y K and Jeffries J R 2016 *Phys. Rev. B* **93** 094511
- [25] Zhu J et al 2013 *Sci. Rep.* **3** 2016
- [26] Cai S et al 2018 *Phys. Rev. Mater.* **2** 114203
- [27] An C, Chen X, Wu B, Zhou Y, Zhou Y, Zhang R, Park C, Song F and Yang Z 2018 *Phys. Rev. B* **97** 174516
- [28] He T et al 2019 *Phys. Rev. B* **100** 094525
- [29] Qi X-L and Zhang S-C 2011 *Rev. Mod. Phys.* **83** 1057
- [30] Sato M and Ando Y 2017 *Rep. Prog. Phys.* **80** 076501
- [31] Bay T V, Naka T, Huang Y K, Luigjes H, Golden M S and de Visser A 2012 *Phys. Rev. Lett.* **108** 057001
- [32] Nikitin A M, Pan Y, Huang Y K, Naka T and de Visser A 2016 *Phys. Rev. B* **94** 144516
- [33] Zhou Y et al 2016 *Phys. Rev. B* **93** 144514
- [34] Smylie M P, Willa K, Ryan K, Claus H, Kwok W-K, Qiu Y, Hor Y S and Welp U 2017 *Physica C* **543** 58
- [35] Werthamer N R, Helfand E and Hohenberg P C 1966 *Phys. Rev.* **147** 295
- [36] Scharnberg K and Klemm R A 1980 *Phys. Rev. B* **22** 5233
- [37] Li M et al 2019 *Phys. Rev. B* **100** 224521
- [38] Du G et al 2017 *Nat. Commun.* **8** 14466
- [39] Kurter C et al 2019 *Nano Lett.* **19** 38
- [40] Han C Q et al 2015 *Appl. Phys. Lett.* **107** 171602
- [41] Liu Z, Yao X, Shao J, Zuo M, Pi L, Tan S, Zhang C and Zhang Y 2015 *J. Am. Chem. Soc.* **137** 10512
- [42] Shruti M V K, Neha P, Srivastava P and Patnaik S 2015 *Phys. Rev. B* **92** 020506
- [43] Li M, Fang Y, Pei C, Qi Y and Wang L 2020 *J. Phys.: Condens. Matter.* **32** 385701
- [44] Manikandan K et al 2017 *Europhys. Lett.* **118** 47008
- [45] Sun J P et al 2016 *Nat. Commun.* **7** 12146
- [46] Sun L et al 2012 *Nature* **483** 67
- [47] Sun J P et al 2018 *Nat. Commun.* **9** 380
- [48] Pauwvonder L J 1958 *Philips Res. Rep.* **13** 1
- [49] Prescher C and Prakapenka V B 2015 *High Press. Res.* **35** 223
- [50] Larson A C and Von Dreele R B 2004 General structure analysis system (GSAS) *Los Alamos National Laboratory Report LAUR 86-748*
- [51] Toby B H 2001 *J. Appl. Crystallogr.* **34** 210
- [52] Mao H K, Xu J and Bell P M 1986 *J. Geophys. Res.* **91** 4673
- [53] Chiatti O et al 2016 *Sci. Rep.* **6** 27483
- [54] Cai S et al 2018 *npj Quantum Mater.* **3** 62
- [55] Xu Y et al 2014 *Nat. Phys.* **10** 956
- [56] Hamlin J J, Jeffries J R, Butch N P, Syers P, Zocco D A, Weir S T, Vohra Y K, Paglione J and Maple M B 2012 *J. Phys.: Condens. Matter.* **24** 035602
- [57] Li M T, Fang Y F, Sun Z, Zhang J C and Lin C T 2018 *J. Phys.: Condens. Matter.* **30** 31LT01
- [58] Hor Y S et al 2010 *Phys. Rev. Lett.* **104** 057001
- [59] Kriener M, Segawa K, Ren Z, Sasaki S and Ando Y 2011 *Phys. Rev. Lett.* **106** 127004
- [60] Lawson B J et al 2016 *Phys. Rev. B* **94** 041114
- [61] Machado A J S et al 2017 *Phys. Rev. B* **95** 144505
- [62] Sun Y, Kittaka S, Sakakibara T, Machida K, Wang J, Wen J, Xing X, Shi Z and Tamegai T 2019 *Phys. Rev. Lett.* **123** 027002
- [63] Smylie M P et al 2018 *Sci. Rep.* **8** 7666
- [64] Pan Y, Nikitin A M, Araizi G K, Huang Y K, Matsushita Y, Naka T and de Visser A 2016 *Sci. Rep.* **6** 28632
- [65] Kita T and Arai M 2004 *Phys. Rev. B* **70** 224522
- [66] Almoalem A et al 2021 *Phys. Rev. B* **103** 174518
- [67] Lahoud E et al 2013 *Phys. Rev. B* **88** 195107

- [68] Suderow H, Tissen V G, Brison J P, Martinez J L and Vieira S 2005 *Phys. Rev. Lett.* **95** 117006
- [69] Eltsev Y, Lee S, Nakao K, Chikumoto N, Tajima S, Koshizuka N and Murakami M 2002 *Phys. Rev. B* **65** 140501
- [70] Kaluarachchi U S, Taufour V, Böhmer A E, Tanatar M A, Bud'ko S L, Kogan V G, Prozorov R and Canfield P C 2016 *Phys. Rev. B* **93** 064503
- [71] Kogan V G and Prozorov R 2012 *Rep. Prog. Phys.* **75** 114502
- [72] Jaccard D, Wilhelm H, Alami-Yadri K and Vargoz E 1999 *Physica B* **259–261** 1
- [73] Lin X, Fauqué B and Behnia K 2015 *Science* **349** 945
- [74] McMillan W L 1968 *Phys. Rev.* **167** 331
- [75] Yu Z, Wang L, Hu Q, Zhao J, Yan S, Yang K, Sinogeikin S, Gu G and Mao H-k. 2015 *Sci. Rep.* **5** 15939
- [76] Birch F 1947 *Phys. Rev.* **71** 809
- [77] Xi X, Ma C, Liu Z, Chen Z, Ku W, Berger H, Martin C, Tanner D B and Carr G L 2013 *Phys. Rev. Lett.* **111** 155701
- [78] Bera A, Pal K, Muthu D V S, Waghmare U V and Sood A K 2016 *J. Phys.: Condens. Matter.* **28** 105401
- [79] Vilaplana R et al 2011 *Phys. Rev. B* **84** 184110
- [80] Qiu Y, Sanders K N, Dai J, Medvedeva J E, Wu W, Ghaemi P, Vojta T and Hor Y S 2015 arXiv:1512.03519
- [81] German R, Komleva E V, Stein P, Mazurenko V G, Wang Z, Streltsov S V, Ando Y and van Loosdrecht P H M 2019 *Phys. Rev. Mater.* **3** 054204
- [82] Sohler T, Ponomarev E, Gibertini M, Berger H, Marzari N, Ubrig N and Morpurgo A F 2019 *Phys. Rev. X* **9** 031019
- [83] Zhang A et al 2019 *Phys. Rev. B* **100** 201107
- [84] Zhang A et al 2019 *Phys. Rev. B* **100** 060504
- [85] Li G et al 2019 *Phys. Rev. Mater.* **3** 023601
- [86] Ueda K, Kaneko R, Subedi A, Minola M, Kim B J, Fujioka J, Tokura Y and Keimer B 2019 *Phys. Rev. B* **100** 115157
- [87] Hadjiev V G, Zhou X, Strohm T, Cardona M, Lin Q M and Chu C W 1998 *Phys. Rev. B* **58** 1043
- [88] Yue L, Ren X, Han T, Guo J, Wu Z, Zhang Y and Li Y 2017 *Phys. Rev. B* **96** 180505
- [89] Köhler H and Becker C R 1974 *Phys. Status Solidi b* **61** 533
- [90] Richter W and Becker C R 1977 *Phys. Status Solidi b* **84** 619
- [91] Saha K, Légaré K and Garate I 2015 *Phys. Rev. Lett.* **115** 176405
- [92] Born M and Oppenheimer R 1927 *Ann. Phys.* **389** 457
- [93] Mazin I I 2019 *J. Phys.: Condens. Matter.* **31** 174001
- [94] Tomita T, Hamlin J J, Schilling J S, Hinks D G and Jorgensen J D 2001 *Phys. Rev. B* **64** 092505
- [95] Hopfield J J 1971 *Physica* **55** 41
- [96] Hanfland M, Beister H and Syassen K 1989 *Phys. Rev. B* **39** 12598
- [97] Abstreiter G, Cardona M and Pinczuk A 1984 *Light Scattering in Solids IV* ed M Cardona and G Güntherodt (Berlin: Springer)
- [98] Friedl B, Thomsen C and Cardona M 1990 *Phys. Rev. Lett.* **65** 915
- [99] Proust C, Vignolle B, Levallois J, Adachi S and Hussey N E 2016 *Proc. Natl Acad. Sci. USA* **113** 13654
- [100] Fang Y, You W-L and Li M 2020 *New J. Phys.* **22** 053026
- [101] Chen X et al 2011 *Appl. Phys. Lett.* **99** 261912
- [102] Willa K, Willa R, Song K W, Gu G D, Schneeloch J A, Zhong R, Koshchev A E, Kwok W-K and Welp U 2018 *Phys. Rev. B* **98** 184509
- [103] Yonezawa S 2019 *Condens. Matter* **4** 2
- [104] Wan X and Savrasov S Y 2014 *Nat. Commun.* **5** 4144
- [105] Wang J et al 2019 *Nat. Commun.* **10** 2802
- [106] Kuntsevich A Y, Bryzgalov M A, Akzyanov R S, Martovitskii V P, Rakhmanov A L and Selivanov Y G 2019 *Phys. Rev. B* **100** 224509
- [107] Levy N, Zhang T, Ha J, Sharifi F, Talin A A, Kuk Y and Stroschio J A 2013 *Phys. Rev. Lett.* **110** 117001